Supporting Information

Multi-material 3D printed eutectogel microneedle patches integrated with fast customization and tunable drug delivery

Huan Liu, Xinmeng Zhou, Aminov Nail, Hao Yu, Zilian Yu, Yue Sun, Kun Wang, Nanbin Bao, Decheng Meng, Liran Zhu and Huanjun Li*

Key Laboratory of Cluster Science of Ministry of Education, Key Laboratory of Medical Molecule Science and Pharmaceutics Engineering of Ministry of Industry and Information Technology, School of Chemistry and Chemical Engineering, Beijing Institute of Technology, 100081, Beijing, China

***Corresponding Author**: Huanjun Li. lihj@bit.edu.cn

Contents

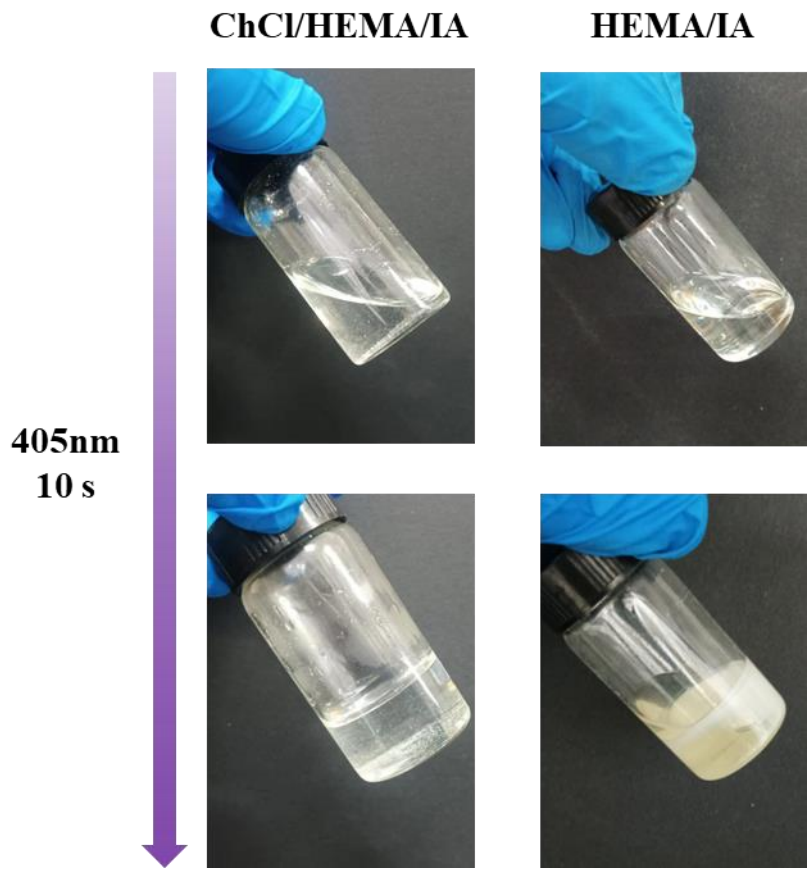

Fig. S1 Photographs showing the catalytic effect of ChCl for photopolymerization.

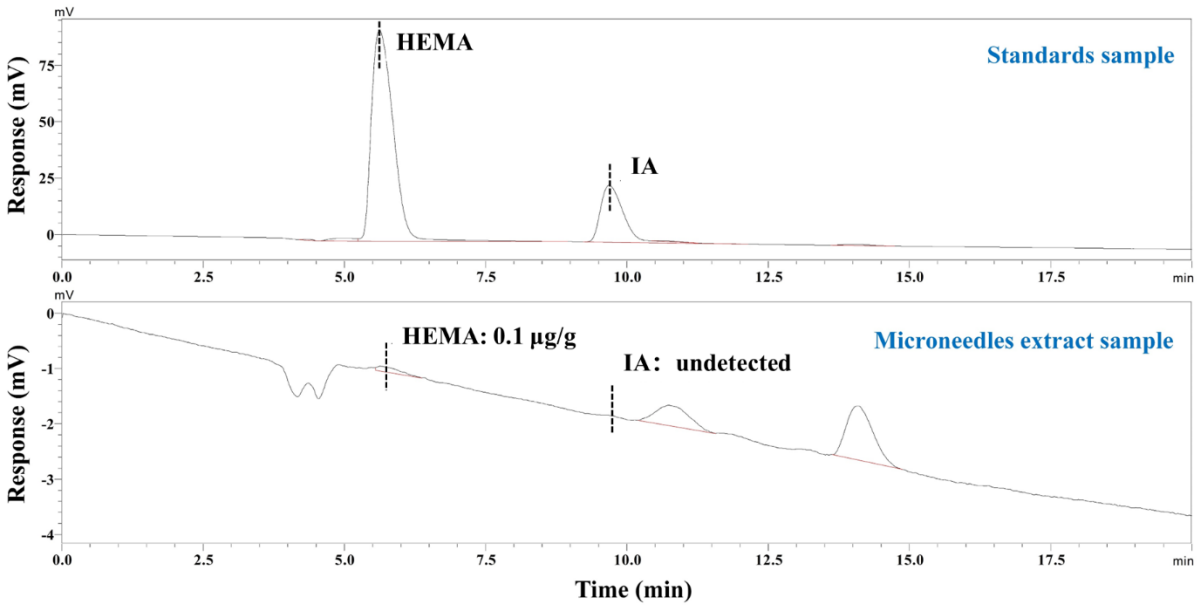

Fig. S2 HPLC quantitative detection chromatogram of HEMA/IA residual monomer.

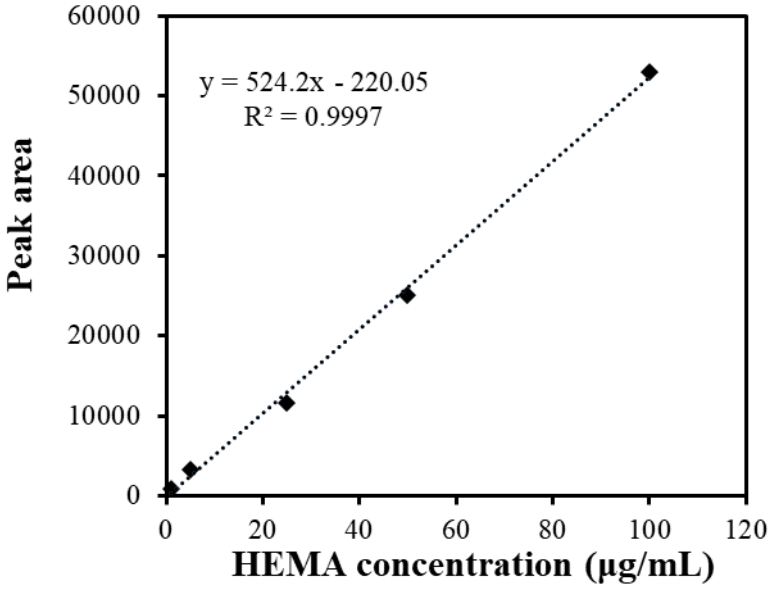

Fig. S3 HPLC quantitative detection standard curve of HEMA concentration.

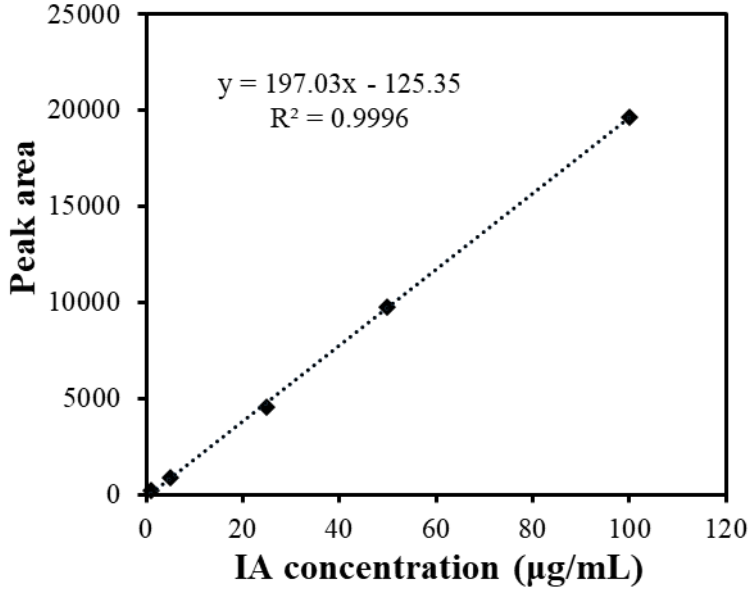

Fig. S4 HPLC quantitative detection standard curve of IA concentration.

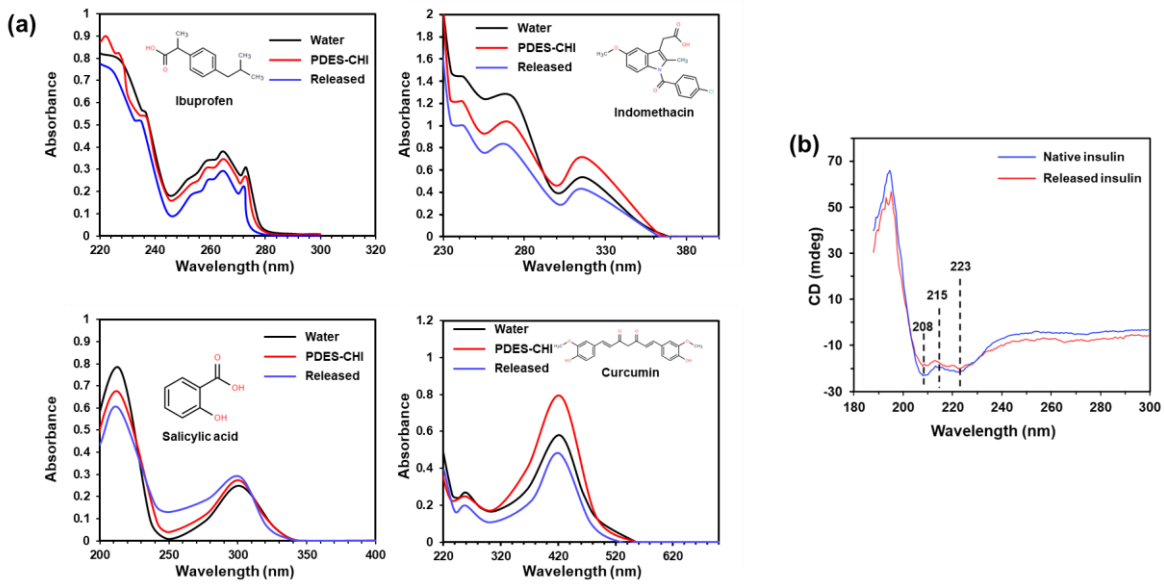

Fig. S5 The structural stability of (a) four hydrophobic APIs and (b) insulin after the photopolymerization of PDES.

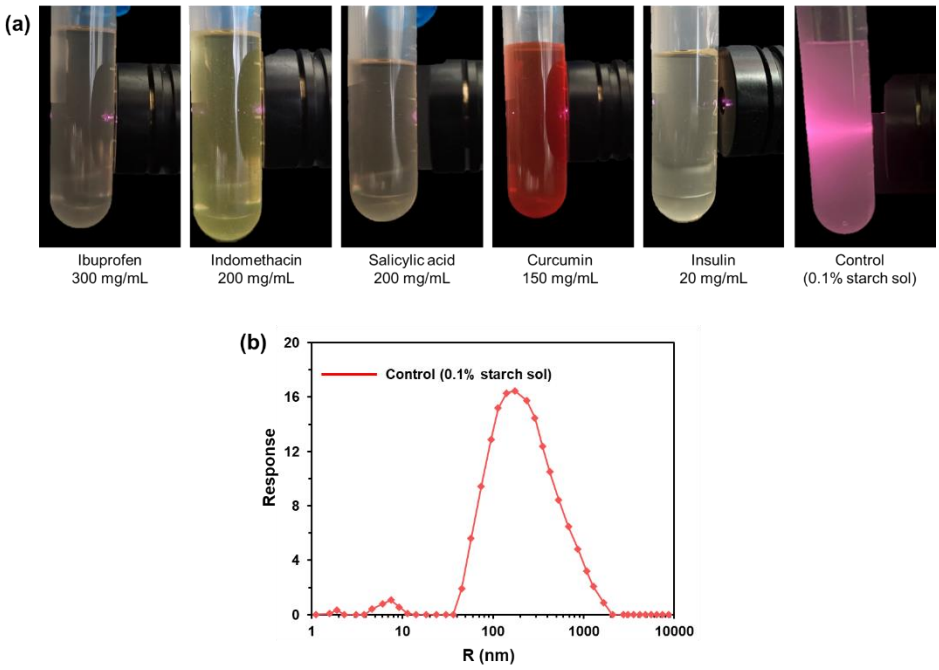

Fig. S6 Illustration of hydrophobic drugs in CHI-PDES system: (a) Tyndall effect of different APIs in CHI-PDES; (b) Size distribution of the colloidal particles in DES.

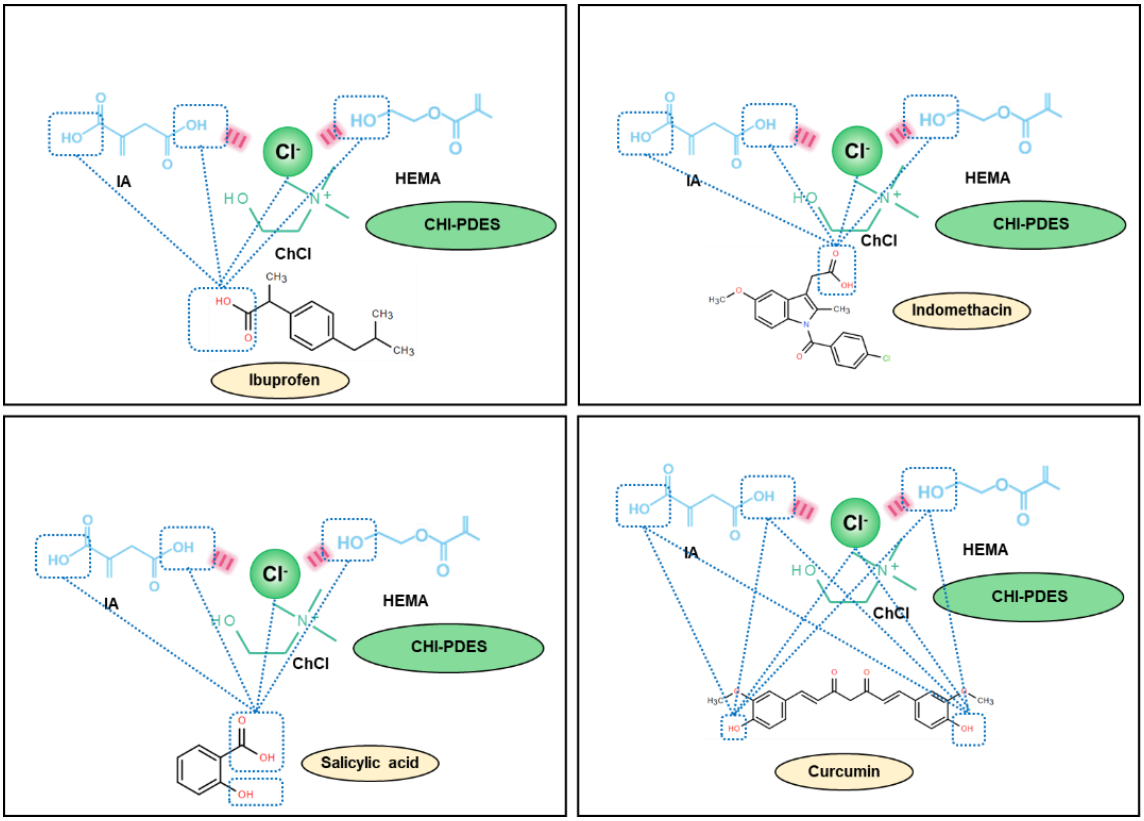

Fig. S7 Solvent-solute interactions between the hydrophobic drugs and CHI-PDES (H-bonding interactions).

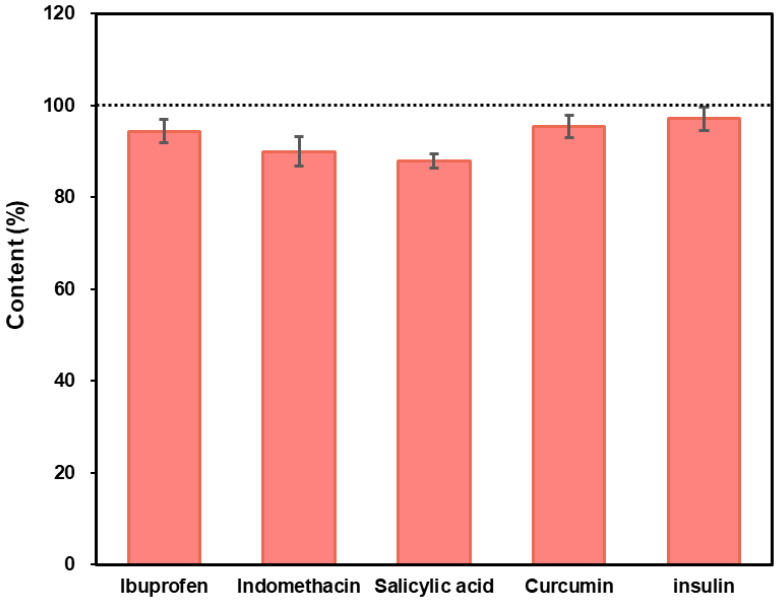

Fig. S8 The content stability of APIs after the photopolymerization of PDES.

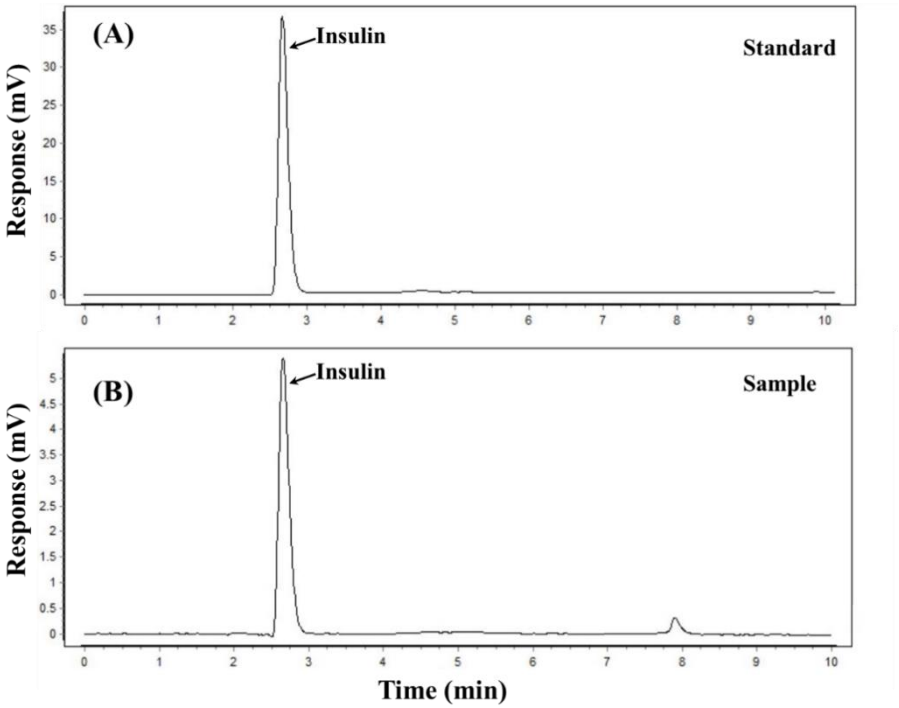

Fig. S9 Insulin HPLC quantitative detection chromatogram. (**A**) Standard sample. (**B**) Experimental sample.

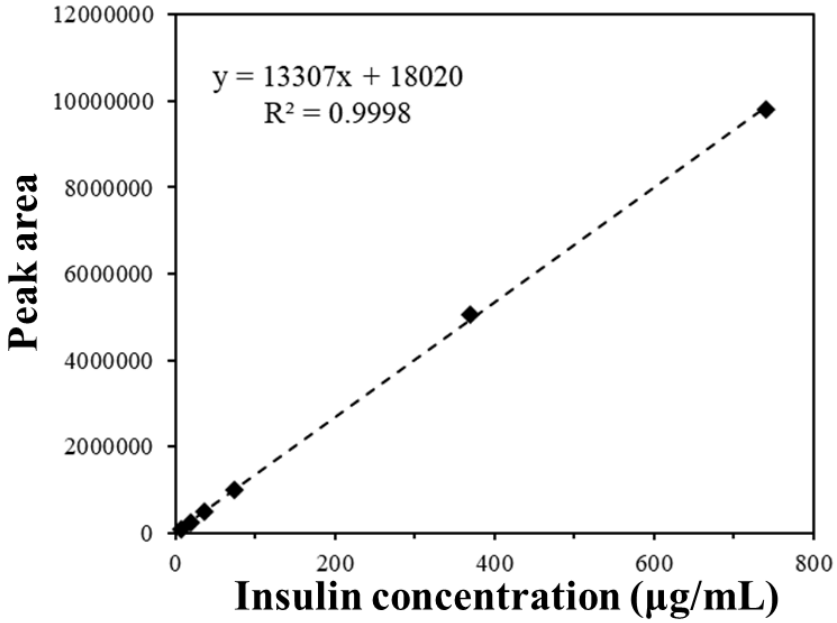

Fig. S10 HPLC quantitative detection standard curve of insulin.

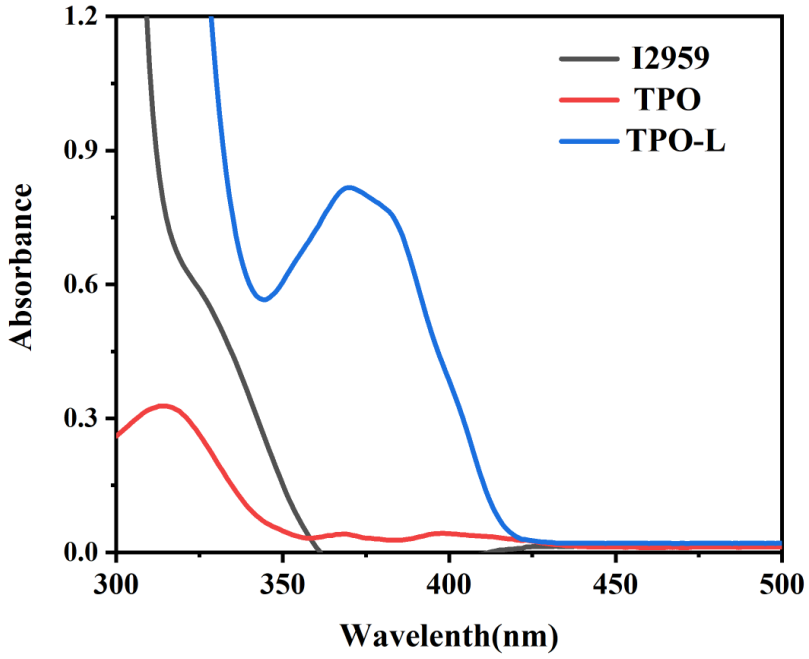

Fig. S11 UV absorption wavelength curves of different photoinitiators.

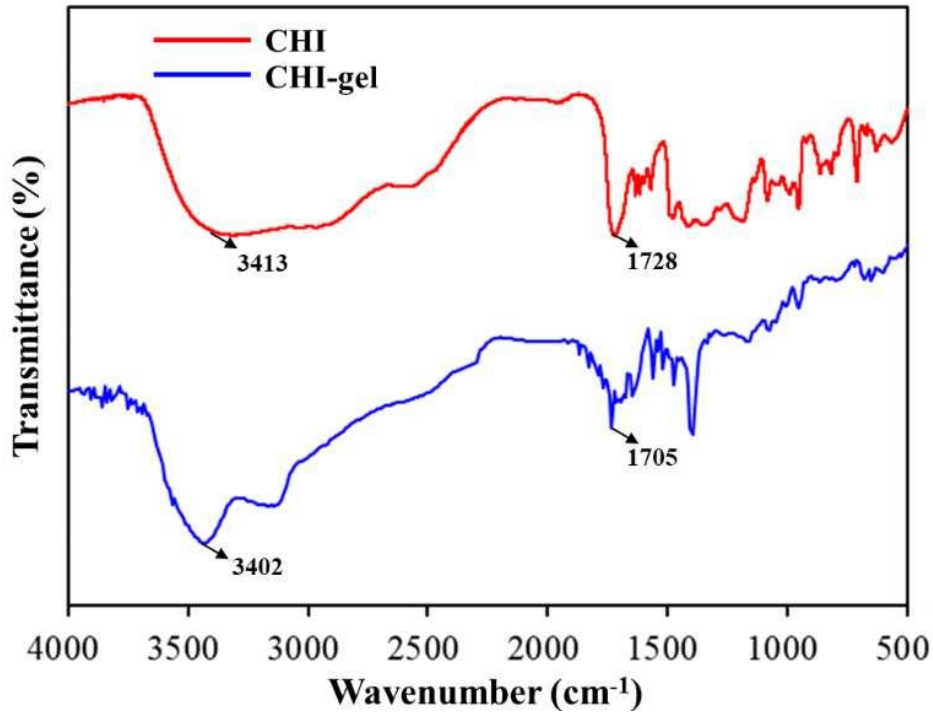

Fig. S12 FTIR characterization of needle portion eutectogel material.

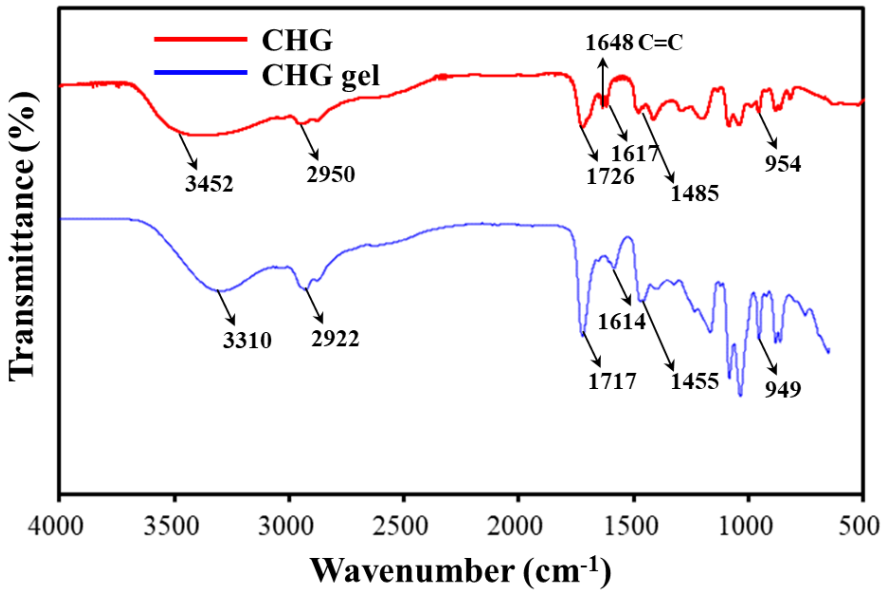

Fig. S13 FTIR characterization of backing layer eutectogel material.

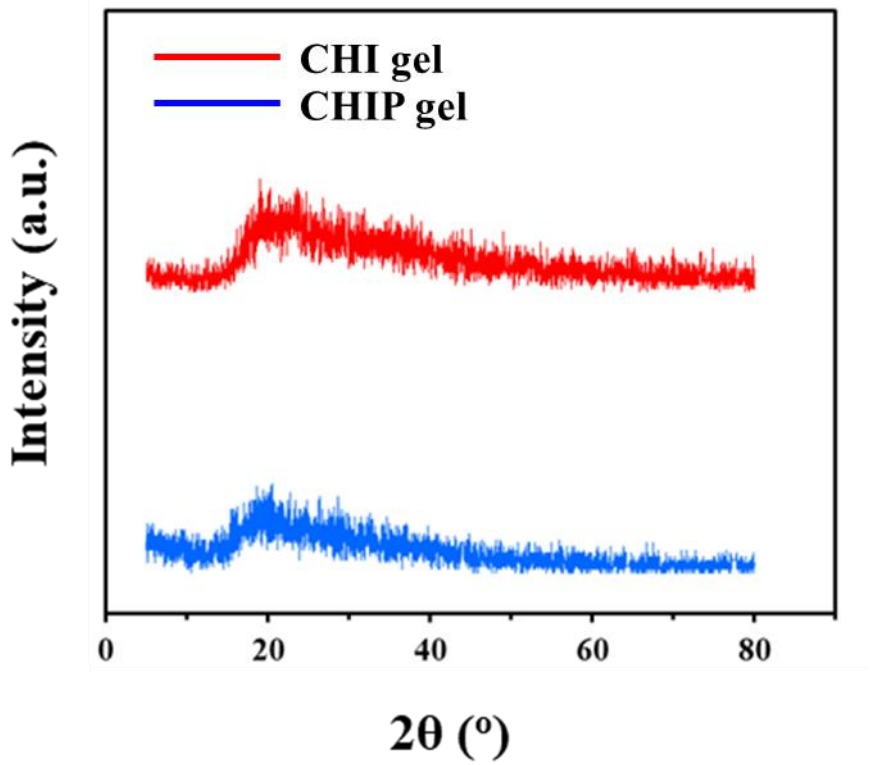

Fig. S14 XRD characterization of needle portion eutectogel material.

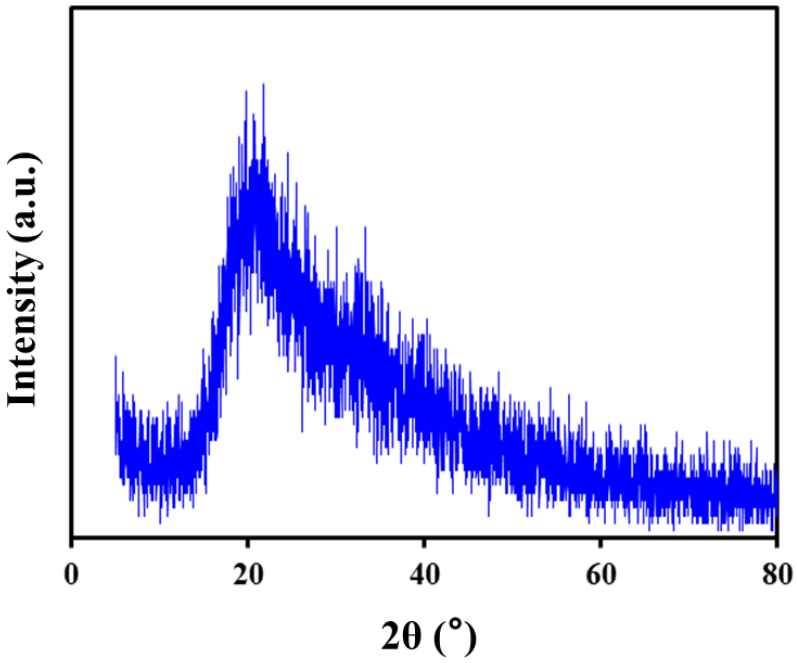

Fig. S15 XRD characterization of backing layer eutectogel material (CHG gel).

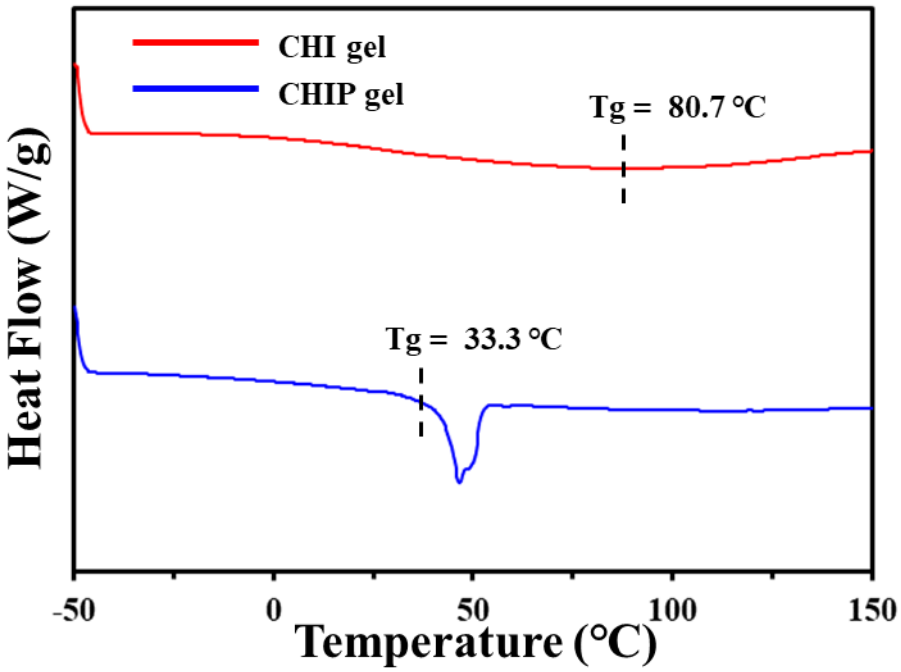

Fig. S16 DSC characterization of needle portion eutectogel material.

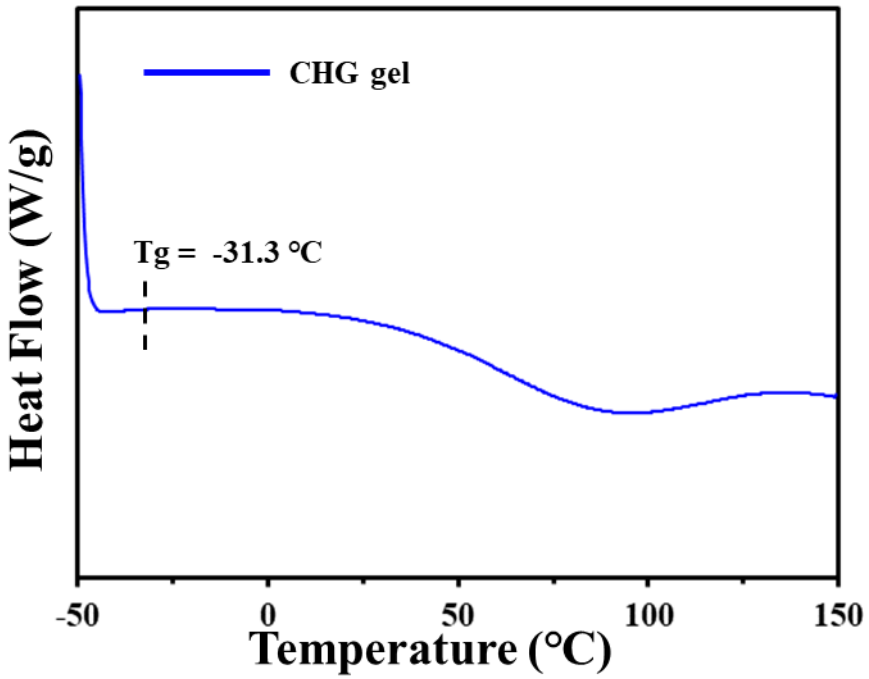

Fig. S17 DSC characterization of backing layer eutectogel material.

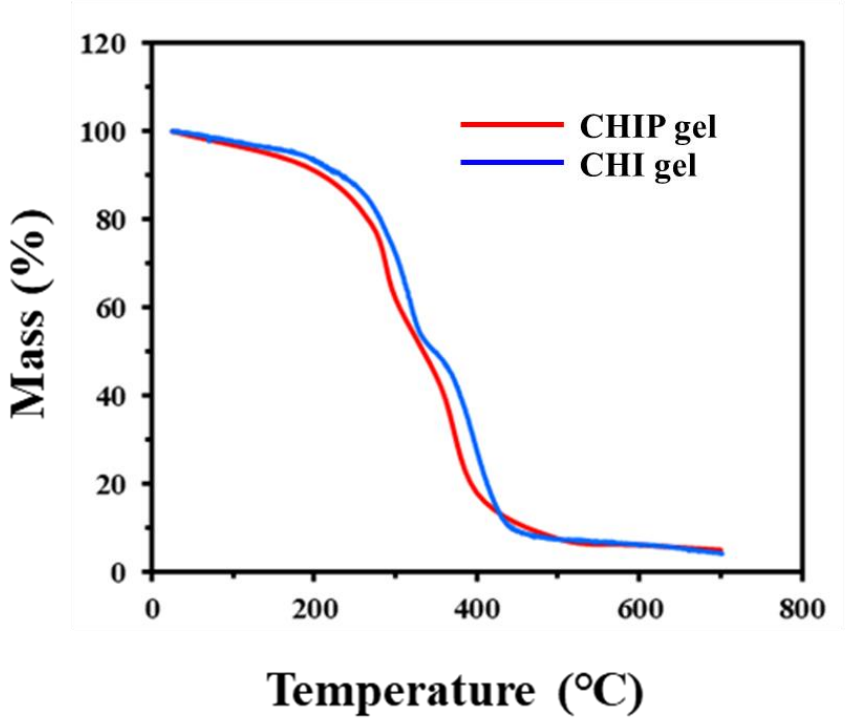

Fig. S18 TGA characterization of needle portion eutectogel material.

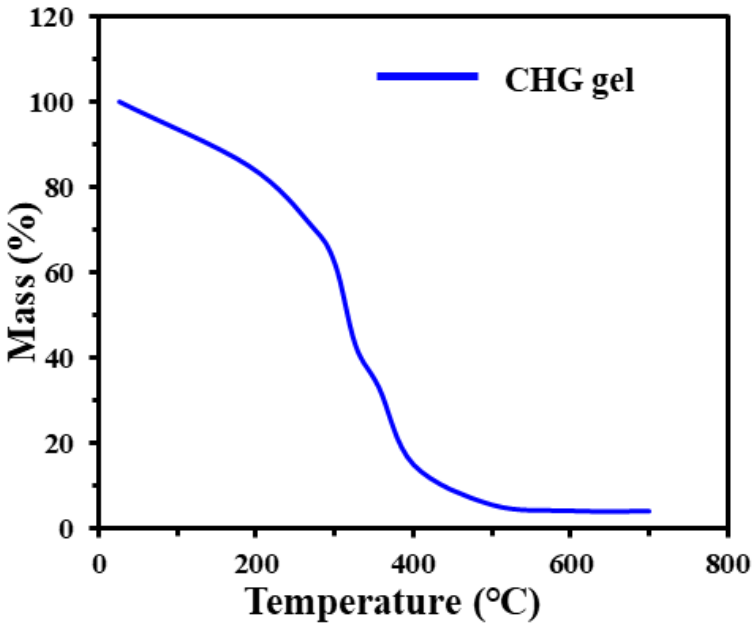

Fig. S19 TGA characterization of backing layer eutectogel material (CHG gel).

Fig. S20 Photograph showing conductive effect of eutectogel MNs.

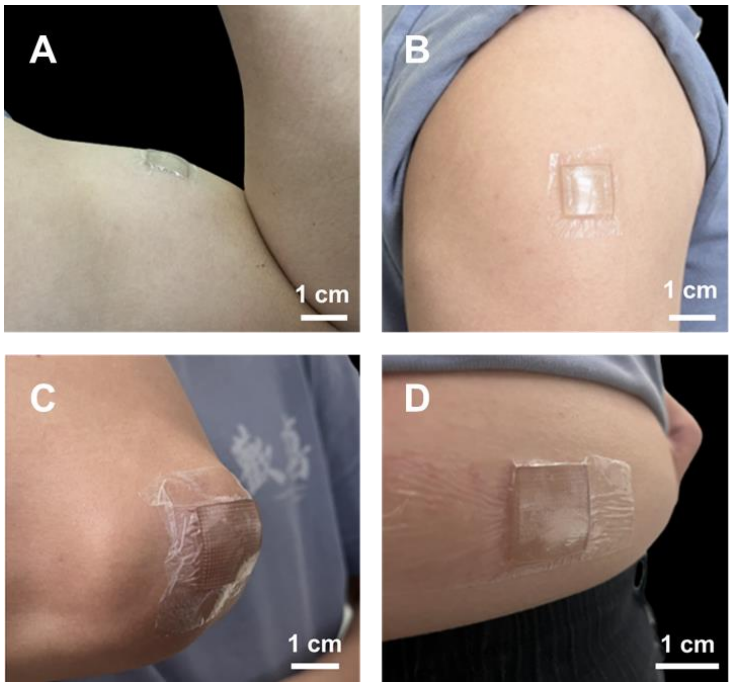

Fig. S21 Flexible, stretchable MN backing layers for different parts of the body. (A) Inside arm. (B) Outside arm. (C) Elbow joint. (D) Abdomen.

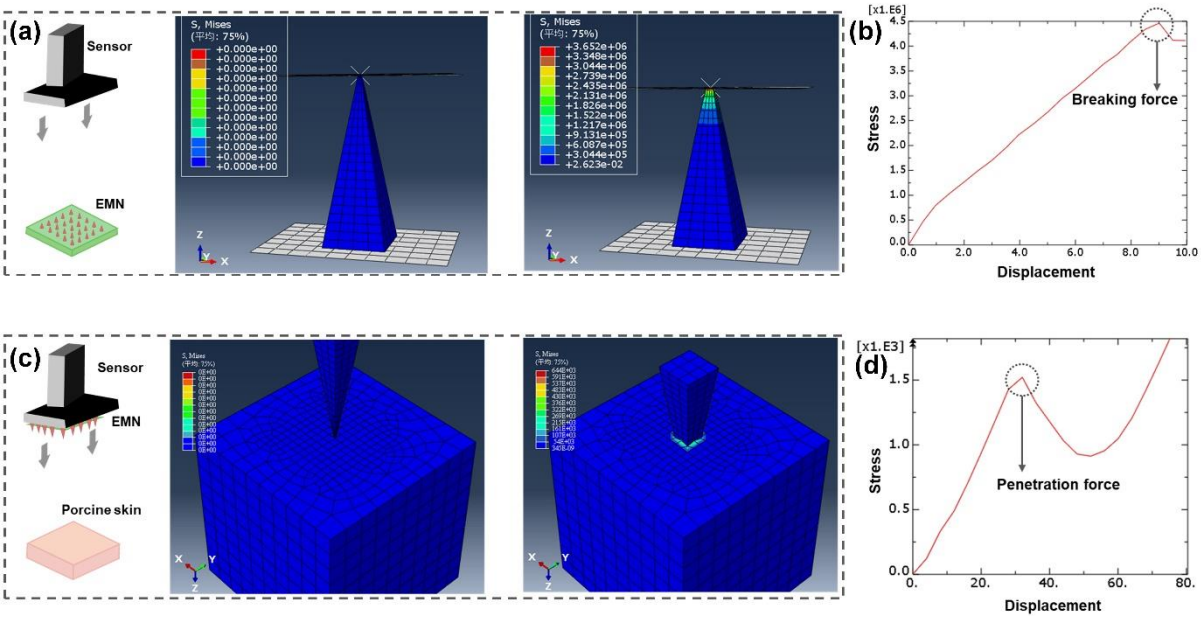

Fig. S22 Optimizing the structural design of EMNs combined by simulation and experimental approaches. (a) FEA of MN breaking force test process. (b) Stress-strain curve under MN breaking force by FEA. (c) FEA of MN penetration force test process. (d) Stress-strain curve under MN penetration force by FEA.

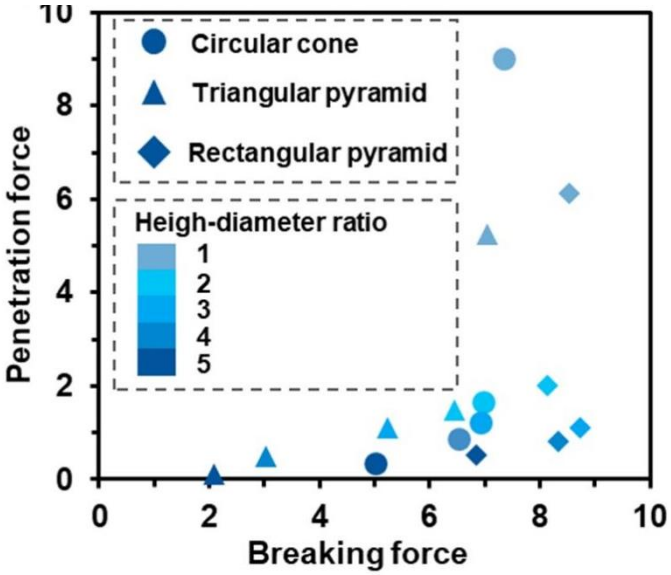

Fig. S23 The evaluation of the geometric parameters of EMNs by FEA.

Fig. S24 The recovery of human skin after MN acupuncture.

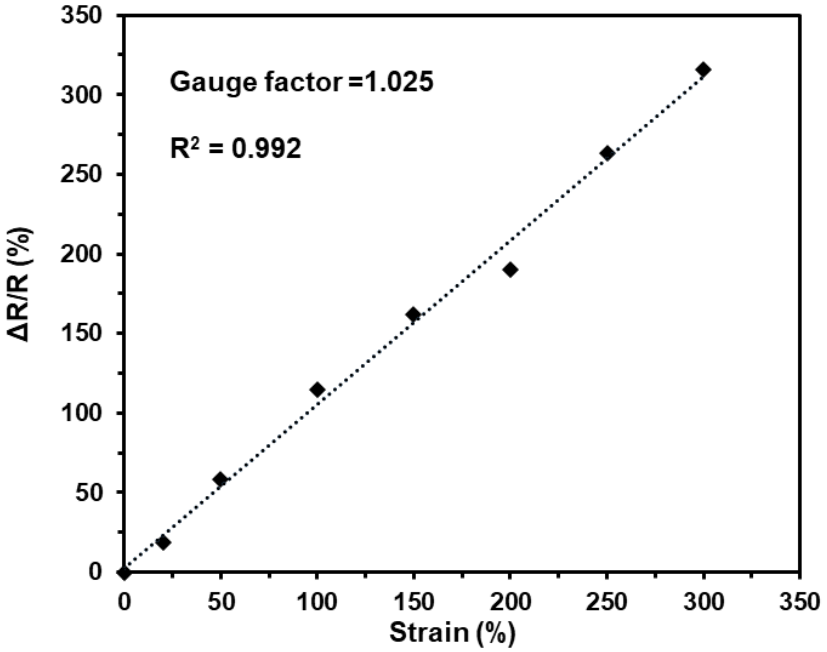

Fig. S25 Relative resistance changes of EMNs sensor as a function of tensile strain.

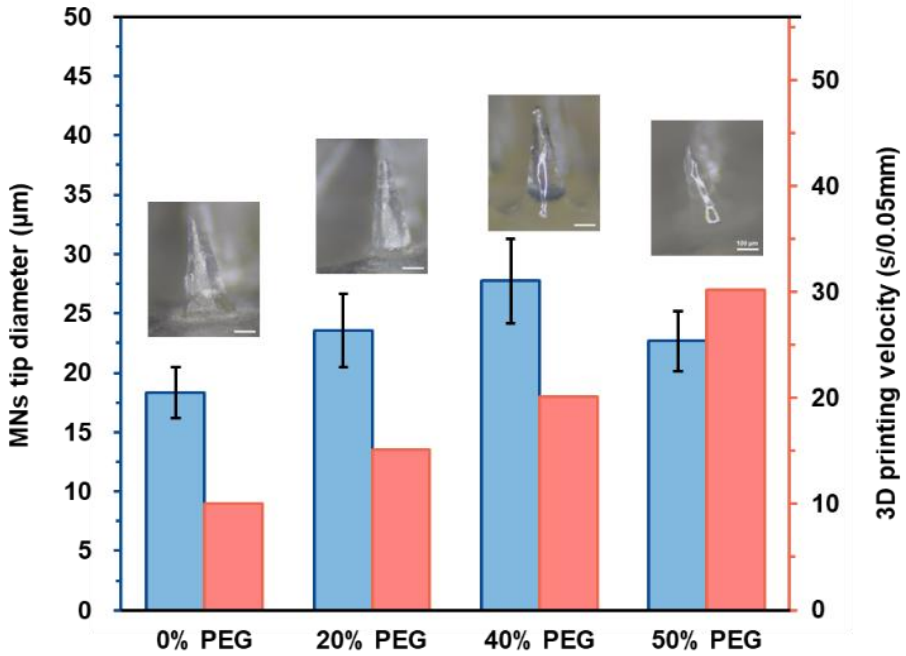

Fig. S26 The resolution of EMN with different contents of PEG1500 and 3D printing velocity.

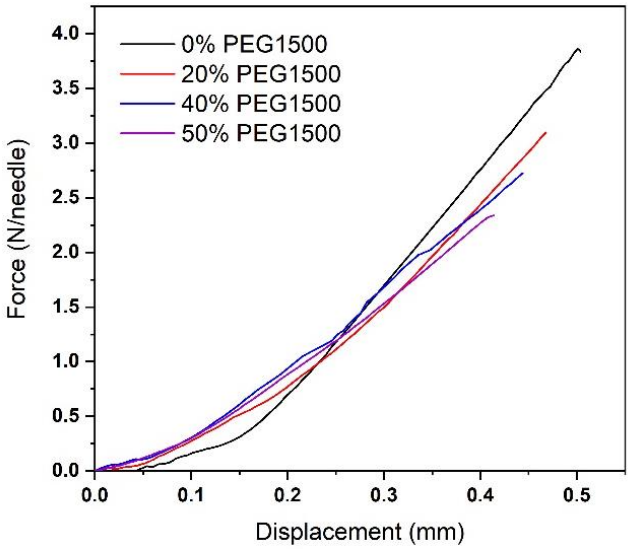

Fig. S27 The mechanical strength of EMNs with different contents of PEG1500.

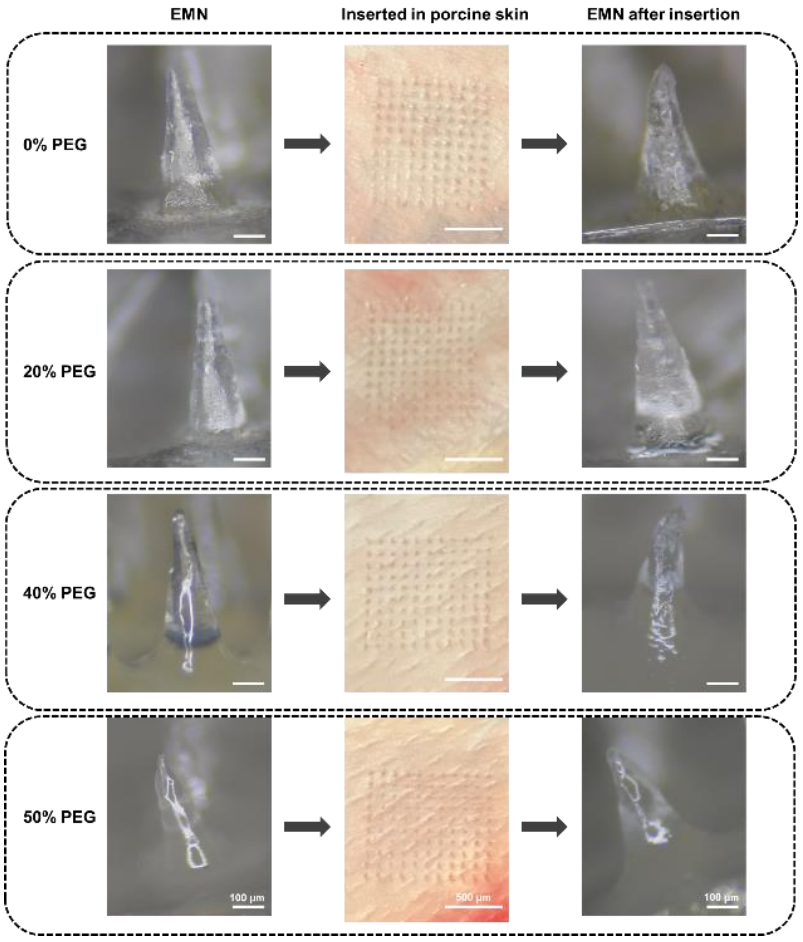

Fig. S28 Micrograph of EMN and porcine skin in the process of insertion.

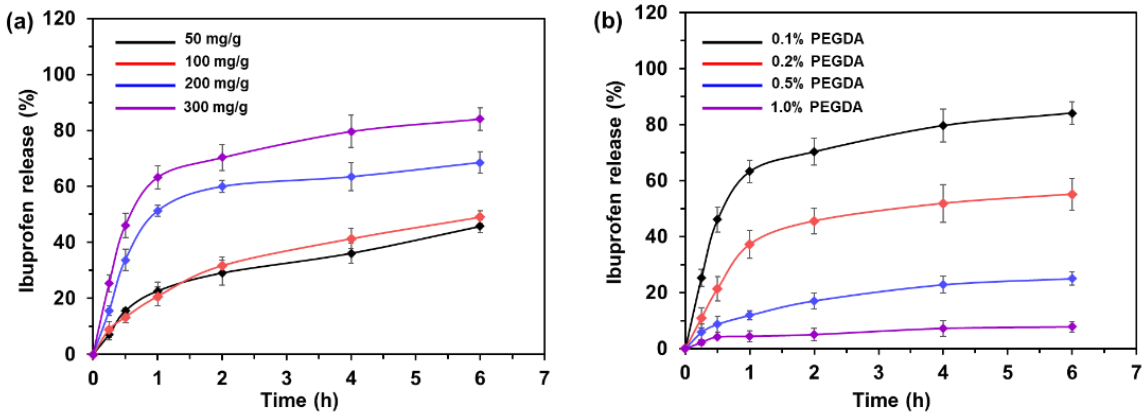

Fig. S29 Drug release profile of EMNs with different drug-loaded (a) and content of crosslinker (b).

Tab. S1 Formulation of various PDESs.

DES monomer	MN backing layer /g	IR-MN needle portion /g	XR-MN needle portion /g
ChCl	2.39	2.12	2.12
HEMA	4.46	5.91	5.91
IA	0	1.97	1.97
glycerol	3.15	0	0
PEG1500	0	2	4
PEGDA	0.01	0.012	0.014
TPO-L	0.01	0.012	0.014

Tab. S2 Conductivity analysis of eutectogel MNs.

PDES	Electrical Conductivity (mS/cm)
ChCl/HEMA/IA (CHI)	0.23
ChCl/HEMA/IA/PEG (CHIP)	0.15
ChCl/HEMA/glycerol (CHG)	61.42

Tab. S3 Pharmacokinetic parameters following subcutaneous injection of insulin and administration of extended-release and immediate-release insulin-loaded eutectogel MN in diabetic rats.

Group	AUC $_{0\text{-}12}$(μU/L*h)	C_{max}(μU/L)	MRT $_{0\text{-}12}$(h)	T_{max}(h)
S.C.injection	238 .24±6.18	124.44±25.15	1.57±0.25	1.00±0.00
IR-MNs	189.58±24.69	86.71±13.63	2.22±0.29	2.00±0.00
XR-MNs	171.98±28.62	27.67±8.78	6.16±0.37	4.67±0.94

Tab. S4 Price of one insulin-loaded eutectogel MN patch (1 cm × 1 cm, 0.5 g).

Ingredient	Weight (g)	Unit price (US cents /g)	Price (US cents)
ChCl	0.23	1.48	0.34
HEMA	0.12	1.42	0.17
IA	0.02	1.77	0.04
glycerine	0.11	0.85	0.09
PEG1500	0.02	0.71	0.01
Insulin	1.5×10^{-3}	212.70	0.32
Total prices	NA	NA	0.97

Tab. S5 Finite element simulation parameters for MN modeling.

Skin structure	Thickness (μm)	Elasticity modulus (Mpa)	Possion ratio	density (g/cm^3)
Cuticula	20	1.00	0.39	1200
Stratum epidermis	70	0.50	0.45	1100
Dermis	1500	0.06	0.47	1100

Tab. S6 Finite element simulation parameters for Skin modeling.

Type	Elasticity modulus (Mpa)	Possion ratio
MN backing layer	0.11	0.45
MN body layer	76.42	0.23